Enhanced Localized Surface Plasmonic Resonances in Dielectric Photonic Band-Gap Structures: Fabry-Perot Nanocavities & Photonic Crystal Slot Waveguides

Dihan Hasan, and Alan X. Wang *
School of Electrical Engineering and Computer Science, Oregon State University, Corvallis, OR, 97331
*Corresponding author: wang@eecs.oregonstate.edu

ABSTRACT

We describe approaches to enhance localized surface plasmons by placing metallic nanoparticles into two different structures: (i) Fabry-Perot (F-P) resonant cavities, and (ii) Photonic crystal slot waveguides. Through synchronization of the plasmonic and resonant modes, electric field at the surface of the nanoparticles is enhanced by a factor of 4~20 compared with the nanoparticles in free space, depending on the device structure and coupling mechanism. We report key differences between the F-P enhancement and the slow-light enhancement to the plasmonic effect in details. This theoretical investigation reveals a new method to strengthen plasmonic resonances and suggests that the sensitivity of existing plasmonic sensors can be further improved if they are integrated with dielectric resonant photonic devices.
Keywords: Microcavities, Optical sensing and sensors, Photonic Crystal Slot, Surface plasmons.

1. INTRODUCTION

Localized surface plasmons (LSPs) from metallic nano-particles (NPs) have attracted tremendous research interests because they are capable of concentrating light beyond the diffraction limit, which leads to extremely strong local electric field at the metal-dielectric interface. LSPs play significant roles in numerous applications including label-free biomedical sensing [1], optical tweezers by utilizing near-field coupling between NPs [2], and light-trapping for photovoltaic devices [3]. For example, LSPs have increased the sensitivity of surface-enhanced Raman scattering (SERS) that is enough for single-molecule detection [4-5], as the single-molecule enhancement factor is proportional to the fourth power of the localized electric field amplitude in the hot spots [6]. Two methods have been adopted to maximize the electric field of the LSPs. The most popular one focuses on optimization of size, shape, separation and distribution of metallic NPs [7-8]. The second approach is based on increasing power density of the incident light [9]. For example, a high numerical aperture lens can be used to focus a laser beam into a small spot ($\lambda/2$ is the theoretical limit and λ is the wavelength), which effectively enhance the optical power density in the lateral plane (the plane that is perpendicular to the Poynting vector). In this paper, we describe a third approach to amplify LSPs by placing a metallic (Ag or Au) NP in two different dielectric photonic band gap (PBG) structures. The electric field enhancement in the FP cavity comes from the constructive interference of the standing waves inside the resonant structure, which can increase the intensity of the excitation light through longitudinal (the direction parallel to the Poynting vector) compression. On the other hand, the Photonic Crystal (PC) slot waveguide can provide strong field enhancement in the slot region due to the slow-light effect if the device is carefully designed and integrated with advanced coupling structures. The approach we discuss here not only achieves much higher field enhancement, but also suggests an integrated solution to improve performance of on-chip plasmonic sensors. We must point out that, although the single-particle-in-device structure is difficult to implement as a practical device, the analysis here will pave the way to explain the interaction of resonant modes of photonic crystal device with complex plasmonic modes of array like metal structures with highly dense number of hotspots fabricated either by the self-assembly technique or thermal annealing of metal films. Nevertheless, techniques of performing single metal object spectroscopy have been proposed recently in different literatures [9]. The approach described in this work has already been theoretically and experimentally confirmed on more engineering-feasible structure like guided-mode-resonant (GMR) gratings coated with metallic nanoparticles [10-11]. Such Purcell-like enhancement is a function of both quality factor and mode volume of the device of interest [12]. In this work, we conduct a comparative theoretical study on the enhancement of LSPs due to the F-P resonance and the slow-light effect and demonstrate device-specific schemes to increase the strength of LSP resonances which will eventually improve the efficiency of plasmon-enhanced optical devices.

Photonic and Phononic Properties of Engineered Nanostructures III,
edited by Ali Adibi, Shawn-Yu Lin, Axel Scherer, Proc. of SPIE Vol. 8632, 863203
 · doi: 10.1117/12.2005549

2. THEORETICAL BACKGROUND

Figure 1 (a) and (b) shows the schematic diagrams of the F-P-cavity and the photonic crystal slot waveguide. The F-P cavity is formed by alternating dielectric pairs of 99 nm SiO_2 (n=1.45)/ 69 nm Si_3N_4 (n=2.02) with five pairs for the front mirror and seven pairs for the back mirror. The waveguide width of the DBR mirrors is 400nm for single mode operation. The length of the air cavity is 295 nm, which gives a single longitudinal resonant mode at 540 nm wavelength with peak electric field in the center of the cavity. The input light is a Gaussian-shape transverse-magnetic (TM) source with normalized peak electric field amplitude of E_0=1. The electric field enhancement factor EF is defined as E_{max}/E_0 throughout this analysis, and E_{max} is the peak electric field in a given region. In Figure 1 (b), the Si_3N_4 PC slot device has a waveguide width of 127 nm. The air holes in the active region have a diameter of 82.5 nm and are distributed at a period of 254 nm. The slot width has been fixed at 60 nm.

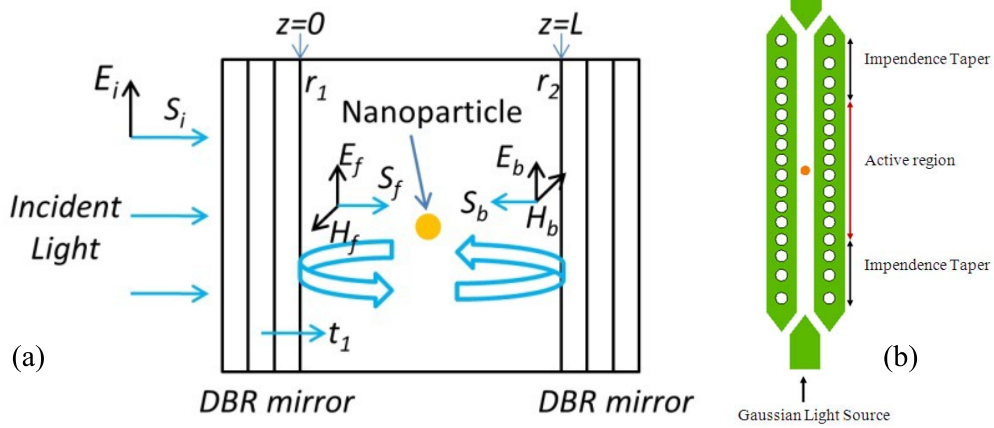

Figure 1. Schematic of (a) An Optical Resonant Cavity formed by two DBR mirrors (b) 1-D slotted Photonic Crystal Waveguide (PCW) with additional coupling structures: optical mode converter and impedence taper

In Figure 2 (a), the simulated electric field distribution inside the resonant cavity obtained by a 3D frequency domain solver is shown [13]. It can be clearly observed from the preliminary simulation that, the electric field amplitude inside the cavity is around 8.5× the input normalized beam during resonance. This additional enhancement can be effectively coupled with plasmonic enhancement to improve the strength of Raman signal of the sample under investigation during SERS.

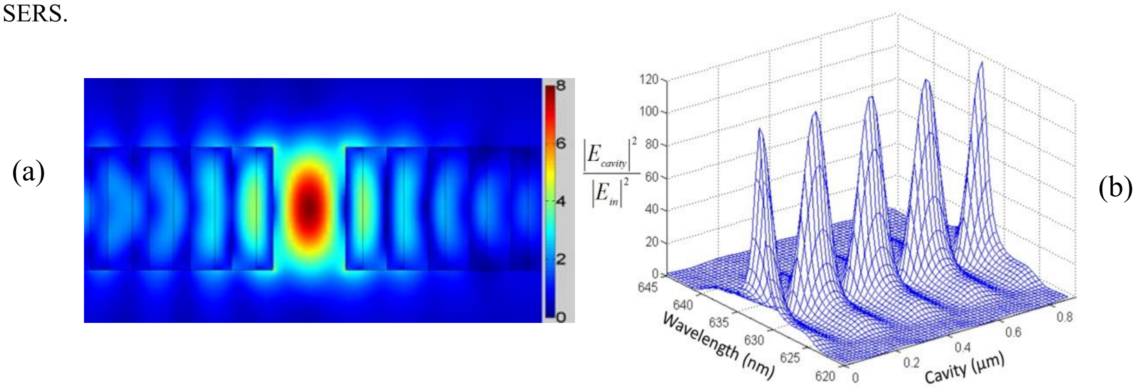

Figure 2. (a) 2D electric field enhancement distribution inside the resonant cavity at 540 nm obtained by finite element (FE) simulation (b) Analytically obtained optical intensity distribution inside the resonant cavity.

In fact, resonant cavity structure has been used to improve the performance of various photonic devices for a long time [14]. The enhanced electric field inside the cavity is formed by two oppositely propagating waves with strong coherence. The standing waves inside a resonant cavity can be written as:

$$E = E_f + E_b = E_f(0)\exp(-j\beta z) + E_b(L)\exp[j\beta(z-L)] \quad (1)$$

where L is the length of the cavity, r_1 and r_2 are the amplitude reflectivity ($R_1=r_1^2$, $R_2=r_2^2$, R_1 and R_2 are the intensity reflectivity), E_f is the forward traveling field, E_b is the back reflected field from the mirror, and β is the propagation constant. The optical intensity inside the resonant cavity, which is proportional to $|E|^2$ is given as:

$$I \propto |E|^2 = \left\{ \frac{\left|1-r_1^2\right|}{\left|1-r_1 r_2 e^{j(2\beta L+\psi_1+\psi_2)}\right|^2} \right\} \times [1 + r_2^2 + 2r_2 \cos(2\beta(L-z)+\psi_2)] \cdot |E_{in}|^2 \quad (2)$$

where Ψ_1 and Ψ_2 are the phase shift induced by the front and back mirrors, respectively. The standing wave patterns inside the cavity as a function of the wavelength are shown in Figure 2 (b). For example, if the reflectivity of the DBR mirrors is 98.3%, the peak optical intensity is nearly 100× stronger than that of the incident light.

In the slotted PC waveguide, the electric field enhancement occurs in the narrow slot region while the group velocity of the propagating light in the medium decreases significantly. Hence, such structure can be used to strengthen the light matter interaction for different purposes [15]. The dispersion diagram of the designed PC slot waveguide obtained using a planar-wave-expansion (PWE) method is illustrated in Figure 3(a). We focus on the narrow band gap as marked in the figure which has a significant portion below the light line. It is obvious that, at band edge wavelength the group velocity will become minimum and metal-light interaction will be maximized .However, we observed some deviation between the results obtained using PWE and the finite element (FE) based field solver. One possible reason is the PWM assumes the structure to be infinitely long whereas we consider only 30 periods of air holes. We obtained a peak enhancement wavelength at 632 nm in our FE simulation which is a little bit smaller than the band edge wavelength from PWE simulation. The simulated electric field distribution in the slot region at this wavelength considering an effective slab index of 2 is illustrated in Figure 3(b). It can be observed from Figure 3(b) that, the electric field distribution follows a standing wave pattern which is governed by the periodicity of the 1D photonic crystal structures on both side. We also do an investigation at 662 nm where the band-gap is located. It is clearly visible that, the field enhancement in the active region of the device at this point is 5 times smaller than at 632 nm which is because there is no transmission and slow-light effect at 662 nm. To get a better picture of the slow-light effect, we have also shown the field distribution at the input ends of the device in Figure 3(d) and (e). The enhancement observed at 662 nm at the interface of the mode converter and the PC-slot waveguide is because of the strong reflection of light by the active region at this wavelength.

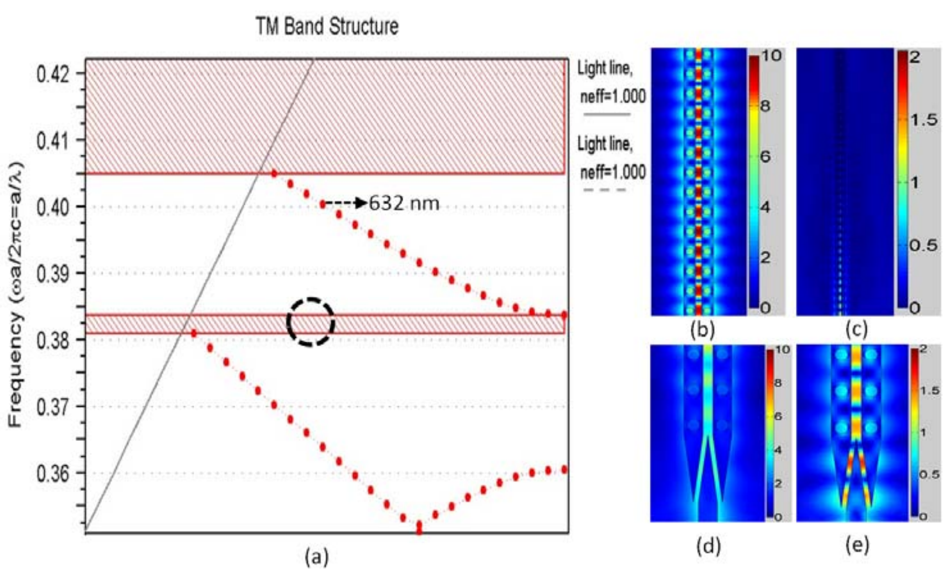

Figure 3. (a) Photonic band-gap diagram of the Si_3N_4 PC slot waveguide obtained by Bandsolve, RSOFT. The band-gap under consideration is marked (b) Electric field distribution inside the slot region at (b) 632 nm and (c) 662 nm (nearly zero transmission). Electric field distribution at the input end at (d) 632 nm (e) 662 nm.

To simplify the analysis of additional improvement of plasmonic enhancement by metals inside the resonant structure, we have considered 2D models of simulation instead of 3D here. However, in reality, plasmonic behavior of metal nanostructures is strongly influenced by their 3D shapes. To address this issue and justify the outcomes of our work, we have run a numerical experiment on aspect ratio (height (h)/diameter (d)) dependence of field enhancement by metal nanorod. It is to be noted here that, during the FE simulation, meshing grids have been increased to at least 10 elements per wavelength and the convergence of EFs is achieved. The refractive indices of the metal are given by Drude-Lorentz model to incorporate dispersion [16]. It can be observed from Figure 4(a) that, at higher aspect ratio, resonance behavior of nanorod becomes nearly insensitive to wavelength variation in addition to the drastic reduction of field enhancement at the surface. In this simulation, the light source was assumed to excite the rod structure from the side instead from the top with a polarization perpendicular to the axis. In our 2D model, the metal nanoparticle (NP) can be assumed to be an infinite aspect ratio nanorod structure. Hence, we can ignore the strong wavelength dependence of metal NPs and focus primarily on the additional enhancement that can be achieved from the optical devices under consideration. Besides, it can be seen in Figure 4(b) that, at this extreme condition, Au-nanorod will provide larger field enhancement than Ag--nanorod within the range of wavelength considered. This also implies larger extinction cross section of Au structure that may introduce more perturbation into the physics of the two optical devices. In Figure 5, the simulated field profiles are shown considering a TM-polarized light source. The width of the Gaussian beam was set to 400 nm for the FP cavity simulation. However, we considered a 127 nm wide Gaussian beam during the PC waveguide simulation and scaled the magnitude of the field enhancement accordingly so that both the enhancements for a given NP size remain comparable.

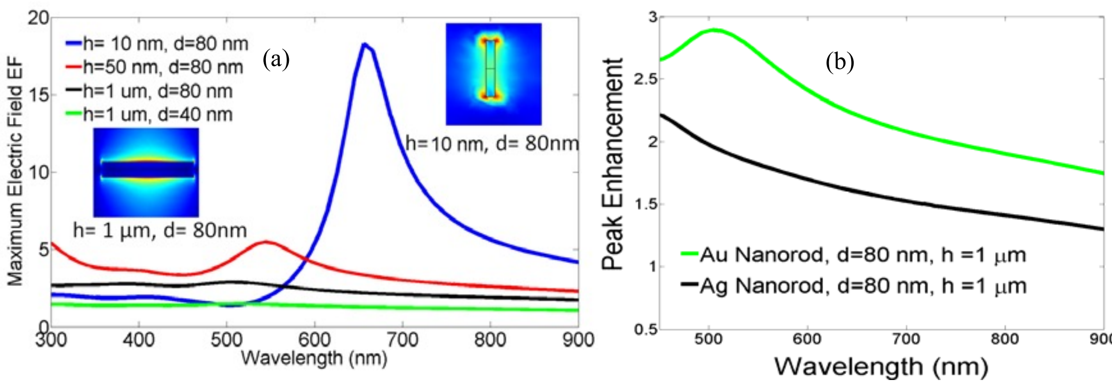

Figure 4. (a) Effect of Ag nanorod aspect ratio and diameter on enhancement spectrum (b) Comparison between peak field enhancements by Au and Ag- nanorod at an aspect ratio of 12.5

(a)

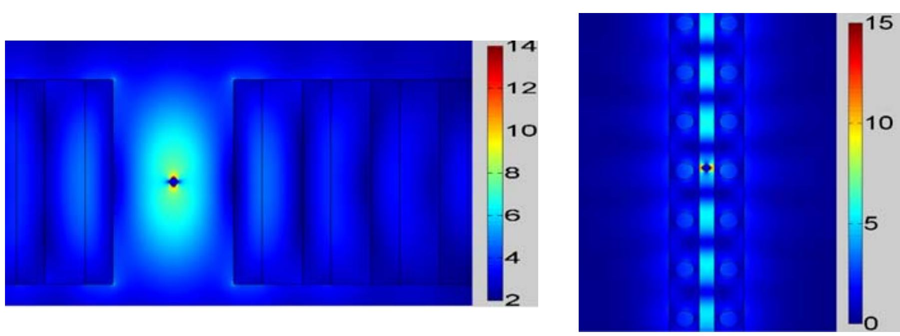

(b)

Figure 5. 2D field enhancement by an 35 nm Ag NP (a) inside the resonant FP-cavity (540 nm) (b) inside the slot region of the PC waveguide (632 nm)

It is clearly visible that field enhancement by Ag NP can be improved at least 7 times when it is placed inside the active region of any of the devices. However, further improvement can still be achieved by tuning the device parameters and operating at the resonant condition. A rigorous analysis of the underlying physics of this phenomenon are going to be performed in the later section.

3. RESULTS AND ANALYSIS

When metallic NPs are placed inside the resonant structure as shown in Figure. 5(a) and 5(b), we expect two major effects. First, metallic NPs extinct (scatter and absorb) the standing waves. It is obvious that such loss of optical power will lower the Q-factor of the resonant cavity and reduce the optical transmission. Second, if the diameter of the NPs is not negligible (>10nm), quadrupole and other higher order resonances appear in the NPs, which will induce phase retardation to optical waves [17-18]. This phase retardation, which depends on the size, shape and position of the NPs, red-shift (to longer wavelength) the resonant frequency of the cavity, and thus it is important to synchronize the LSPs and the resonant cavity to maximize the electric field enhancement factor (EF). Although standing waves inside the resonant cavity can enhance surface plasmons as enhanced plane waves can do, we must point out their slight differences in physics. Standing wave differs itself with plane wave in that there is a $\pi/2$ phase difference between the electric field and the magnetic field. For example, at the point with peak electric field, the magnetic field is actually zero. For plasmonic resonances, we neglect the effect of the magnetic field if the permeability of the material $\mu_r=1$. Therefore, LSPs of metallic NPs see no difference between standing waves and plane waves if the size of the NP is much smaller than the wavelength ($d<\lambda/10$). But if the size of the NP is not negligible, the electric field variation along the longitudinal direction becomes important. The electric field distribution in Figure. 5(a) and 5(b), is a mixture of the resonant mode and the optical extinction pattern of a plasmonic NP in free space. Numerical simulation shows that the electric field enhancement EF of the Ag NP in free space and the resonant FP cavity is 2.37 and 7.5, respectively. Therefore, the standing waves inside the resonant cavity provide 5.9× additional EF to LSPs compared with free space. However, due to the optical absorption of the metallic NP at optical frequencies and the red-shift of the resonant frequency caused by the NP, the total electric field enhancement factor, EF is smaller than the product of the individual EF of 7.5×2.37=17.8. Figure. 6(a) shows the maximum electric field enhancement EF as a function of wavelength from 500 to 600nm for different configurations: F-P cavity only, Au NP in free space, Ag NP in free space, Au NP in cavity and Ag NP in cavity. The simulation results clearly prove that the optical resonant FP cavity can significantly enhance the LSPs whereas the presence of metal will red-shift the resonant frequency of the cavity. We can also see that Au NP provides a larger EF and frequency shift of the resonant cavity. This is because the simulated wavelength range is closer to the plasmonic resonance of the infinite aspect ratio Au structure, where stronger electric field and phase retardation can occur. We observed similar behavior for the case of PC-slot waveguide also. Although the two devices are designed for two different wavelength ranges, effect of operating wavelength can be ignored during the comparative analysis of additional enhancement from optical device due to the insignificant wavelength dependence of the infinite aspect ratio metal structure. In PC slot waveguide, the peak enhancement occurs at the wavelength 632 nm where the group velocity becomes minimum. It can be observed that in Figure 6(b) that, we obtain around 7 times slow-light enhancement from the PC slot waveguide device.

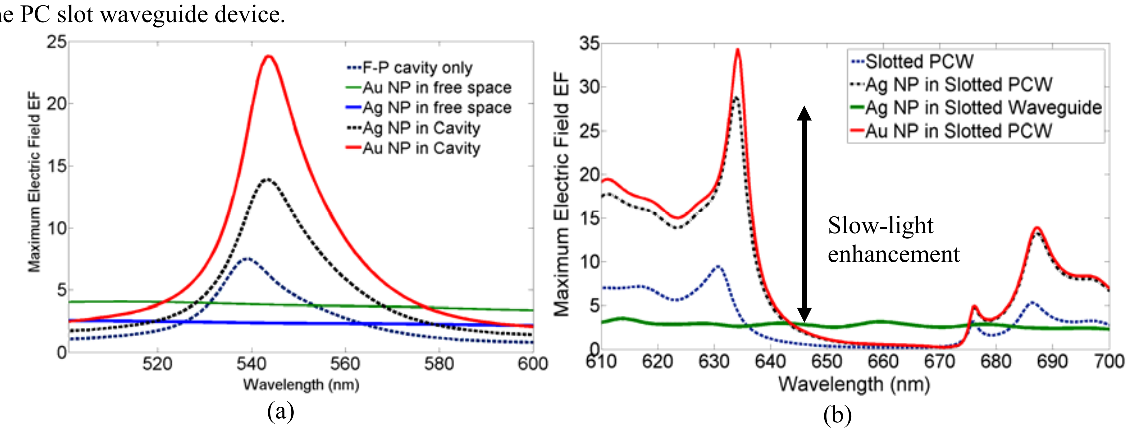

Figure 6. Electric Field enhancement factors (a) FP- cavity (b) Slotted PCW. The metallic NP diameter is fixed at 35 nm.

It is to be noted that, the PC-slot device has another wide band gap above light line at shorter wavelengths as pictured in Figure. 3(a). To observe the effects of radiation losses in this band gap, the device has to be several 100 microns long where as our simulated device is maximum 13 microns long. The peak enhancement observed is also limited by the difficulty of coupling light into the device at slow-light regime [19]. As in FP cavity, we got higher peak enhancement from Au NP as well. In addition to that, the band edge wavelength redshifts with respect to the band edge when there is no nanoparticle. A more detailed investigation on NP size dependence of resonance shift will be conducted later in this section. There are several differences between the properties of enhancement of the two structures. First, the effective contribution from the PC-slot device is larger than the FP device as observed from the maximum EF distribution in Figure 6. This enhancement in the PC-slot structure can be improved further by adding an impendence taper before and after the active region. Second, Q of the complex resonance mode formed due to the mixture of cavity mode and plasmonic mode is relatively higher in PC-slot device. In other words, the enhancement spectrum in the FP device can be treated as a broadband response as compared to the PC-slot which may be useful for a commercial Raman sensor that can detect Raman peaks of sampling material as many as possible. Third, near field coupling mechanism in a more realistic nanoparticle chain structure will be completely different in PC-slot device. We will address the key difference in the end part of this section.

We also investigate the dependence of the electric field EF to the size of the Ag and Au NPs in Figure. 7 (a),(b), (c) and (d). The main peaks around 550nm wavelength originate from the FP cavity resonant mode, where strongest standing waves can excite the LSPs of the metallic NPs. The minor peaks around 650nm wavelength, where the electric field inside the cavity is insensitive to the wavelength because the DBR mirrors lose their functionality due to the low reflectivity, are mainly due to the dipole resonance of the nanoparticles. It is clearly seen that as the diameter of the NPs increases, there will be more red-shift of the resonant frequency. Again, the frequency shift of Au is larger than that of Ag. We must point out that the maximum EF shown in Figure 7 (a) and (b) is the combined effect of the resonant cavity and the NPs with different size. It is not clear whether the change of the EF is due to the standing waves in the resonant cavity or the size of the NPs. In principle, a larger metallic NP should absorb more light and further weaken the standing wave EF of the resonant cavity. But on the other hand, a larger metallic NP has a larger extinction cross section, and thus increases the local electric field at the surface of the metallic NP. In Figure 7 (a), the maximum EF of Ag NPs keeps increasing as the diameter increases from 20nm to 80nm; while in Figure 7 (b), the maximum EF of Au NPs reaches the maximum value when the diameter is around 50nm. This is not difficult to understand as Au has a larger imaginary part of the dielectric constant, which can cause higher absorption loss. Thus the resonant cavity is more sensitive to the size of Au NPs. We observed the similar behavior in PC slot device as illustrated in Figure 7(c) and 7(d). We had to limit the

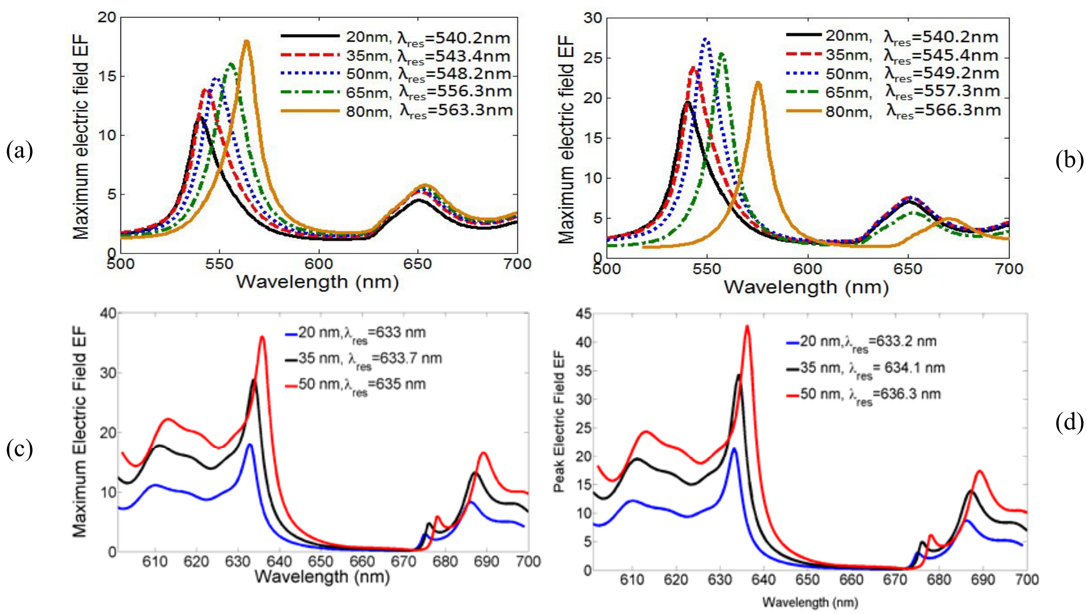

Figure 7. Electric field EF and red-shift of the resonant frequency in presence of NPs with different diameters (a) Ag NP in FP cavity; (b) Au NP in FP cavity (c) Ag NP in PC-slot waveguide (d) Au NP in PC-slot waveguide

the particle size to 50 nm to fit into the slot region during the analysis. It is found that, increasing the size of a single NP always improves the field enhancement within this range. The peak enhancements from both Ag and Au NP in PC-slot device are always greater than in FP cavity regardless of the particle size which clearly demonstrates higher additional enhancement from the PC structure. However, it is interesting that, the resonance shift for larger particle size in FP cavity is more significant than in PC-slot structure. For example, resonance wavelength of the FP structure shifts from

540 nm to 548.2 nm when the particle size is set to 50 nm. On the other hand, it shifts from 632 nm to 635 nm when the particle is placed inside the slot region. One possible explanation is that, the interaction of plasmonic mode and resonant mode of the device is relatively stronger in the FP device. The back and forth travelling wave inside the resonant cavity experiences more phase retardation when the NP volume becomes bigger. We have confirmed this finding in the end part of this section by considering a NP chain at resonance. However, it is still possible to observe additional shift of resonance wavelength when the taper is integrated with the PC-slot device as the interaction between NP mode and the standing wave will be stronger.

We have investigated to overcome the difficulty of coupling light at slow-light regime close to the band edge with a view to improving localized surface plasmons. The main objective was to manipulate the group index of the PC structure gradually from the input end. In this way, there will be effectively less impedence mismatch which will enable to couple the slow-light of high group index into the active region. For doing this, we can either modulate the air hole diameter or the periodicity of the air holes at a given diameter. In this work, we kept the hole size at 82.5 nm and altered the periodicity of the taper region deploying the following exponential equation:

$$P_i = 254 + 13e^{(i-P_{taper})/F},\ \mathrm{P_{taper}} = 12 \qquad (3)$$
$$\mathrm{i=1,2,3,......P_{taper}}$$

We have kept the number of holes in the taper region 12. The spatial distribution of these holes will be determined the modulation factor F. At a very small F, the periodicity of the air holes will nearly become 254 nm which is identical to the case when there is no taper. We can distribute the air holes at different periodicity by setting F to a suitable value. Effect of this parameter has been shown in the inset of Figure 8(a). It can be observed that, at larger F, the modulation of the periodicity becomes slower which implies slower rate of change of group index along the taper region. Following this technique, we simulated the electric field enhancement as a function of F. It can be clearly observed in Figure 8(a) that, the peak enhancement from the single NP can be increased from 28 to 50 as we introduce the taper with F=6.5.

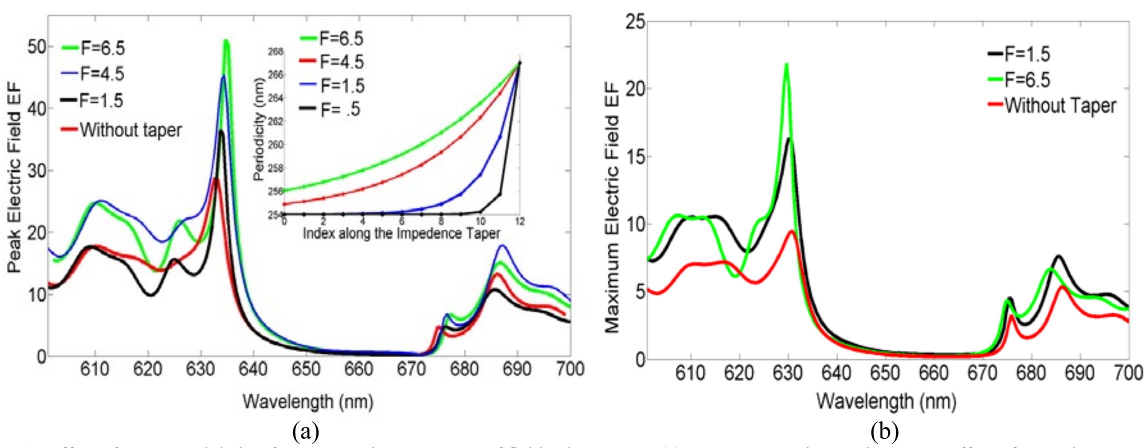

Figure 8. Effect of taper modulation factor, F on improvement of field enhancement (a) 35 nm Ag NP in PC-slot , Inset: effect of F on the distribution of hole periodicity in the taper region (b) PC-slot alone

Such improvement is mainly due to the group index modulation that enables more light to couple into the slot region at band edge wavelength. This additional coupling also increases the magnitude of electric field enhancement in the PC-slot region. We can observe around 3 times improvement when the taper is designed at F=6.5. In addition to the improvement, the resonance wavelength shift becomes more significant as the coupling of light gets stronger. This is quite expected as the interaction between the plasmon mode and the slot mode becomes stronger. In other words, the slot mode experiences more phase retardation than before.

We also investigated the schemes to improve the enhancement due to the localized surface plasmon resonance inside the FP- cavity. Here, we change the reflectivity of the back mirror by increasing the number of stacks. We kept the front mirror periodicity to be 5 like before as increasing it will make it difficult to couple light into the cavity during resonance. In Figure 9(a), the variation of Q as a function of back mirror pair number has been shown. It can be easily understood that, the proposed device is a low Q factor device. It is expected that, the field enhancement will become larger as the Q of the cavity goes higher. Figure 9(b) shows that, the enhancement improves as we increase the back mirror reflectivity. However, it reaches saturation at a certain point as the back mirror reflectivity does not change much beyond that. It is notable here that, the improvement obtained through this technique is not as significant as in the PC-slot device. Also the resonance wavelength shift was found to be less significant during the analysis.

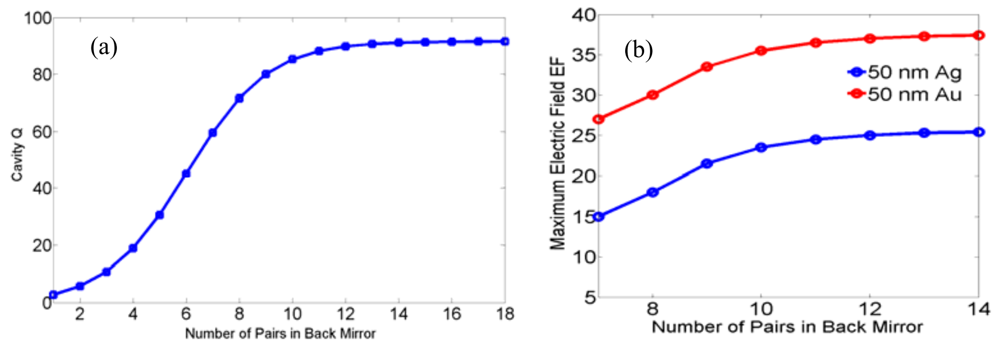

Figure 9. (a) FP-cavity Q as a function of back mirror reflectivity (b) Peak Field enhancement by 50 nm NP as a function of back mirror reflectivity. The peak enhancement has been monitored at the corresponding resonance wavelength.

Later, we studied the plasmonic resonance behavior of NP chain being influenced by the resonant mode of the optical devices under consideration. The NP chain consists of 7 nanoparticles of equal size (50 nm) at gap size of 20 nm to fit into the waveguide region of the cavity. It is to be noted here that, such nanoparticle chain excited by light source with appropriate polarization will exhibit strong near field coupling effect although we are ignoring the effect of coupling into the substrate here. It has been reported in that, such inter-coupling in 1D particle array can lead to narrow line shape resonance with exceptionally large electromagnetic field enhancement [20]. One reason behind the narrow resonance with sharp peak is the coherent interplay arising from multiple scattering by the regularly spaced NPs [21]. In addition to that, such linear chain of NPs can support travelling waves mediated by plasmonic resonance among the elements which may lead to several unusual properties [22]. In this work, we investigate the chain resonance when it is excited by a resonant field instead of a plane wave. In Figure 10(a), the peak enhancement observed along the NP chain inside the FP-cavity has been plotted as a function of wavelength. For Ag system, we did not observe any significant improvement of peak enhancement possibly due to the smaller cross section of individual element. However, the Q of the main resonance becomes much higher than in the single particle system. We observed identical field profiles for both the main resonance and the higher order dipolar resonance as well. It is important to mention here that, the resonance wavelength shifts from

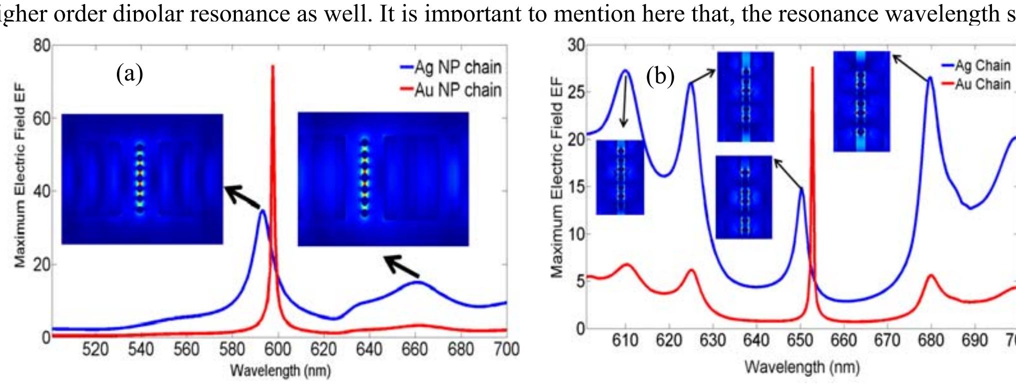

Figure 10 (a) Enhancement spectrum of NP chain inside the (a) FP-cavity (b) PC-slot waveguide. Inset: field profile at different peaks of the spectrum.

540 nm to 590 nm which implies significant amount of phase retardation to the standing wave due to the presence of NP chain. On the other hand, Au NP chain was found to resonate with much stronger field enhancement and sharper Q as shown in Figure. 10(a). The explanation is that, the linear chain of infinite aspect ratio Au structure has large extinction

cross section with resonance peak around the wavelength range under consideration. On the contrary, the PC-slot structure behaves entirely different when NP chain is included. During the analysis, we considered a taper with F=6.5 to ensure the maximum light coupling possible. It is to be kept in mind here that, the device is operating for TM polarization. Hence, the NP chain being considered here cannot demonstrate inter-particle coupling to form the hotspots similar to the case of FP-cavity. It is clearly visible that, the band edge wavelength shifts from 632 nm to 650 nm and 655 nm for Ag and Au chain, respectively. Also the peak enhancement from Ag chain does not occur at the band edge anymore. It is notable here that, the electric field distribution in the slot region follows a standing wave pattern. Hence, the surface enhancement from a NP can occur through coupling of plasmon mode and this standing wave. In other words, the particle chain can be assumed to be excited by a longitudinally polarized light source inside the slot. Hence, the observed enhancement is mainly due to the interaction between single NP resonance and PC-slot resonance. In our simulation, we observed that the location of peak enhancement can change as a function of wavelength. In addition, the effective enhancement from the PC-slot waveguide can reduce due to the damping effect as wave travels through the nanoparticle chain. This can be a reason behind the low enhancement obtained from Ag- chain at band edge. However, the Au-chain demonstrates narrow resonance as in FP-cavity at the band edge wavelength which implies more interaction between the elements of the system. However, the peak enhancement was not too large especially due to the cumulative damping of standing wave inside the slot region. This is a key difference between the underlying physics of the FP-cavity and the PC-slot device. More rigorous theoretical analysis will be conducted in future to address these phenomena. There are also some significant issues from practical point of view. It can be concluded from Figure 10(b) that, the enhancement profile is not uniform inside the PC-slot waveguide as in the FP-cavity shown in Figure 10(a). This implies that the cumulative EF along the chain can be larger when it is integrated with the FP device. Hence, the Raman signal is expected to be stronger when the FP- device is used as a SERS substrate under the same condition. Moreover, it is possible to increase the field enhancement among the particles by several degrees in FP device by reducing the gap size. However, it is not possible in PC-slot waveguide for TM polarization. The only way we can achieve field enhancement in the gap between two elements of the chain considered is the coupling due the travelling wave which will not be as strong as the coupling observed in dimer or trimer like structure for a polarization perpendicular to the gap.

4. CONCLUSION

In conclusion, we have theoretically demonstrated a mechanism to strengthen localized surface plasmon resonance of metal nanoparticles by several times. The approach can be implemented due to recent the advancement of nanofabrication technology like electron beam lithography (EBL) and focused ion beam (FIB) patterning. The key challenge is to precisely integrate the metal structures with the device at the desired location. A method of fabricating 1D NP chain with control over particle size and gap size has been demonstrated by combining the advantage of precise positioning capability of EBL and post deposition thermal annealing [23]. Apart from the fabrication challenges, this method provides a solution to alter the plasmonic behavior of metals in a desired way by tuning the spectral position of the mixed mode resonance. Such spectral manipulation of plasmonic enhancement is of significant engineering merit leading to a highly tunable system for single molecule detection or plasmon enhanced nonlinear optical devices. Performance of FP resonant plasmonic device can also be further improved through a high Q design integrated with efficient coupling mechanism. The merit of the PC-slot waveguide device is crucially limited by the narrow slot width. The slow-light effect in such device can be greatly utilized in structure with wider slot region providing enough room to incorporate metal structures like dimers/trimers which can produce large field enhancement in the hotspots.

5. ACKNOWLEDGEMENT

The authors would like to acknowledge the Faculty Startup Support from the School of EECS at Oregon State University, and the National Institute of Health (NIH) under the Small Business Technology Transfer Research (STTR) program (Grant No. 1R41EB012885-01).

REFERNCES

1. T. Endo, S. Yamamura, N. Nagatani, Y. Morita, Y. Takamura, and E. Tamiya, "Localized surface plasmon resonance based optical biosensor using surface modified nanoparticle layer for label-free monitoring of antigen–antibody reaction," Sci. & Technol. Adv. Mater., 6, 491–500 (2005).
2. K. Wang, E. Schonbrun, and K. B. Crozier, "Propulsion of Gold Nanoparticles with Surface Plasmon Polaritons: Evidence of Enhanced Optical Force from Near-Field Coupling between Gold Particle and Gold Film," Nano Lett., 9, 2623-2629 (2009).
3. H. A. Atwater, and A. Polman, "Plasmonics for improved photovoltaic devices," Nat. Mat., 9, 205-213 (2010).
4. K. Kneipp, Y. Wang, H. Kneipp, L. T. Perelman, I. Itzkan, R. Dasari, and M. S. Feld, "Single molecule detection using surface-enhanced Raman scattering" Phys. Rev. Lett., 78, 1667-1670 (1997).
5. X.-M. Qian and S. M. Nie, "Single-molecule and single-nanoparticle SERS: from fundamental mechanisms to biomedical applications," Chem. Soc. Rev., 37, 912-920(2008).
6. E. C. Le Ru, and P. G. Etchegoin, Principles of Surface-enhanced Raman Spectroscopy (Elsevier, Oxford, 2009).
7. K. L. Kelly, E. Coronado, L. L. Zhao, and G. C. Schatz, "The optical properties of metal nanoparticles: the influence of size, shape, and dielectric environment," J. Phys. Chem., B, 107, 668-677 (2003).
8. D. J. Maxwell, J. R. Taylor, and S. Nie, "Self-Assembled Nanoparticle Probes for Recognition and Detection of Biomolecules," J. Am. Chem. Soc., 124, 9606–9612 (2002).
9. O. Muskens, D. Christofilos, N. D. Fatti and, F. Vall´ee," Optical response of a single noble metal nanoparticle," J. Opt. A: Pure Appl. Opt., 8 264–272,(2006).
10. J. Li, D. Fattal, and Z. Li, "Plasmonic optical antennas on dielectric gratings with high field enhancement for surface enhanced Raman spectroscopy," Appl. Phys. Lett., 94, 263114 (2009).
11. X. Xu, D. Hasan, L. Wang, S. Chakravarty, R. T. Chen, D. L. Fan, and A. X. Wang, "Guided-mode-resonance-coupled plasmonic-active SiO2 nanotubes for surface enhanced Raman spectroscopy," Appl. Phys. Lett., 100, 191114 (2012).
12. A. F. Koenderink, "On the use of Purcell factors for plasmon antennas," Opt. Lett., 35(24), 4208-4210 (2010).
13. http://www.comsol.com/.
14. M. SelimÜnlü, and S. Strite, "Resonant cavity enhanced photonic devices," J. Appl. Phys., 78, 607-640 (1995).
15. W. Lai,S. Chakravarty,X. Wang, C. Lin, and R. Chen,"Photonic Crystal slot waveguide absorption spectrometer for on-chip near-infrared spectroscopy of xylene in water," Appl. Phys. Lett.,98,023304(2011).
16. U. Kreibig, M. Vollmer, Optical properties of Metal Clusters (Springer-Verlag, Berlin, 1995).
17. J. P. Kottmann, and O. J. F. Martin, "Retardation-induced plasmon resonances in coupled nanoparticles," Opt. Lett., 26, 1096-1098 (2001).
18. T. J. Davis, K. C. Vernon, and D. E. Gómez, "Effect of retardation on localized surface plasmon resonances in a metallic nanorod," Opt. Exp., 17, 23655-23663 (2009).
19. C. Lin, A. X. Wang, and R. T. Chen, "Coupling loss minimization of slow light slotted photonic crystal waveguides using mode matching with continuous group index perturbation", Opt. Lett., Vol.37, No.2, pp.232-234 (2012).
20. Y. Chu, E. Schonbrun, T. Yang, and K. B. Crozier, "Experimental observation of narrow surface plasmon resonances in gold nanoparticle arrays,"Appl. Phys. Lett. 93, 181108 (2008).
21. D. Brunazzo, E. Descrovi, and O. J. F. Martin,"Narrowband optical interactions in a plasmonic nanoparticle chain coupled to a metallic film ," Opt. Lett., Vol. 34, Issue 9, pp. 1405-1407 (2009).
22. D. V. Orden, Y. Fainman, and V. Lomakin, "Optical waves on nanoparticle chains coupled with surfaces," Opt. Lett., Vol. 34, Issue 4, pp. 422-424 (2009).
23. Y. Chen, and A. M. Goldman,"Formation of one-dimensional nanoparticle chains," Appl. Phys. Lett. 91, 063119 (2007).